Management and Production Engineering Review
Volume 15 • Number 1 • March 2025 • pp. 1–13
DOI: 10.24425/mper.2025.153923

Multi-Response Optimization of Rotary Electrode EDM Process Parameters for Tungsten Carbide

Ibrahim SABRY[1], Abdel Hamid I. MOURAD[2,3,4], Mohamed ELWAKIL[5], Ahmed M. HEWIDY[1]

[1] *Benha Faculty of Engineering, Benha University / Department of Mechanical Engineering, Egypt*
[2] *Mechanical and Aerospace Engineering Department, College of Engineering, United Arab Emirates University, Al-Ain 15551, United Arab Emirates*
[3] *National Water and Energy Center, United Arab Emirates University, Al Ain 15551, United Arab Emirates*
[4] *On leave from mechanical design department, faculty of engineering, El Mataria, Helwan University, Cairo, Egypt*
[5] *Department of Production Engineering and Mechanical Design, Faculty of Engineering, Tanta University, Tanta, Egypt*

Received: 26 August 2023
Accepted: 19 November 2024

Abstract
Electrical discharge machining (EDM) is a potent technique widely applied to machining materials like EN-8M steel and composite materials. The surface quality achieved through EDM is significantly affected by the settings of its parameters and the type of material being processed. In this context, the focus of research has often been on heavy metals and titanium and magnesium alloys among lighter metals. This study aims to investigate the impact of EDM parameters, specifically on Tungsten Carbide, a material gaining traction across various industries. Our research involved a thorough parametric analysis utilizing a full factorial method to examine factors influencing surface roughness (SR) and material removal rate (MRR). This paper highlights the optimization of MRR using a Rotary electrode attachment. Experiments were conducted employing factorial design to delve deeper into the machining characteristics of Tungsten Carbide with a 4 mm Brass-coated rod as the electrode. Key parameters such as summit current, electrode rotation speed, and Pulse on time were systematically adjusted. The analysis of the machining parameters revealed their significant influence on the outcomes, with p-values falling below 0.05, underscoring their critical role in the EDM process. The developed mathematical models demonstrated a high R-squared value alongside minimal error percentages. The most critical parameters identified for optimal results included an electrode rotational speed of 150 rpm, a summit current of 1.22 A, and a Pulse on time set at 8.45 ms.

Keywords
EDM, factorial analysis, multi-performance.

Introduction

An electrical discharge machine (EDM) is a cutting-edge method used to remove metal through a rapid, high-current electrical discharge between the tool and the workpiece. Unlike traditional machining processes, EDM does not require a larger cutting force. EDM proves particularly useful for machining incredibly tough, electrically conductive materials, such as advanced metals used in aerospace applications. These materials often present challenges for conventional machining techniques, but EDM allows for creating intricate shapes that standard cutting tools struggle to achieve F (Bhaumik & Maity, 2019). This technology is continually finding new applications within the metal-working industry, and it is widely used in the plastics sector to design complex cavities in metal moulds. However, EDM is limited to electrically conductive materials, and EDM can handle them efficiently regardless of their hardness or toughness (Dinesh et al., 2024). Tungsten carbide is a crucial material for tools and dies due to its remarkable hardness, strength, and wear resistance over various temperatures. Its high specific strength makes it difficult to machine using conven-

***Corresponding author**: Abdel Hamid I. Mourad – Mechanical and Aerospace Engineering Department, College of Engineering, United Arab Emirates University, Al-Ain 15551, United Arab Emirates, e-mail: ahmourad@uaeu.ac.ae*

tional methods. However, since electrical discharge machining (EDM) has shown great adaptability when working with tough materials, this process is expected to be effective for tungsten carbide. This highlights the need for detailed research into the impact of various machining parameters on EDM characteristics of tungsten carbide. While there has been a significant amount of study on EDM for composite materials (Lee & Li, 2021), the optimization of EDM conditions (Rao et al., 2014), (Khudhir et al., 2024), and the machinability of ceramics (Naeim et al., 2023), there remains a clear gap in exploring the machining characteristics of tungsten carbide in the context of different machining parameters.

In today's industrial landscape, the significance of durable materials is on the rise, particularly across fields like biomedical, nuclear, defence, aerospace, and automotive sectors. Electric discharge machining is a noteworthy technique for fabricating minute components (Chattopadhyay et al., 2008). Traditional machining processes struggle with hard materials such as Tungsten Carbide due to its exceptional mechanical strength, corrosion resistance, and wear resistance. Consequently, modern machining strategies, including EDM, are gaining traction for handling such tough substances (Amorim & Weingaertner. 2007) EDM is a nontraditional manufacturing method, utilizing electrical discharge energy to erode electrically conductive materials through a thermal process gradually.

Bharti et al. (2010) explored the machining characteristics of Inconel 718 and found that the primary factors impacting material removal rate (MRR) are Peak current and Pulse on time – furthermore, Yan et al. (2000) highlighted the significant effect of polarity on MRR. Chattopadhyay et al. (2008) demonstrated that applying an induced magnetic field to the workpiece during rotational electrical discharge can enhance the material removal rate. In a different study, Chen & Lee (2010) utilized the Taguchi design method to optimize the electrical discharge machining (EDM) parameters for milling aluminium alloy A6061-T6. They assessed surface roughness based on four EDM factors: Pulse current (Ip), pulse-on duration (*Ton*), duty cycle, and machining duration (SR). They employed Analysis of Means (ANOM) and Analysis of Variance (ANOVA) to determine the optimal machining configurations and evaluate each parameter's influence on surface roughness.

Manikandan & Venkatesan (2012) explored the potential of creating micron-sized holes through Micro Electro Discharge Machining (MEDM). Their study focused on how various machining parameters – Ip, *Ton*, and Toff – affected the optimization of key machining characteristics, including Radial Overcut (OC), Material Removal Rate (MRR), and Tool Wear Rate (TWR). Specifically, they examined the machining of Inconel 718 with a brass electrode, employing the Taguchi method for the analysis. The investigation also included a look at the resolidified material surrounding the entrance of the holes and the geometry of the machined micro-holes, with detailed photographs from a scanning electron microscope (SEM) provided to enhance the understanding of their findings.

In a separate study, Chen & Lee (2010) delved into optimizing EDM settings for machining ZrO_2 ceramics. They addressed the challenge of achieving electrical conductivity for the EDM process by applying conductive coatings of adhesive copper and aluminium foils to the non-conductive ceramic surfaces. Using an L27 Orthogonal Array based on the Taguchi design approach, they investigated machining characteristics such as MRR, TWR, and surface roughness (SR). Their results indicated that factors like Ip and pulse length significantly affected MRR and SR, while the adhesive conductive material emerged as the key factor influencing TWR. They also proposed an effective method for moulding electrically non-conductive ceramics that demonstrated excellent efficiency, precision, and surface integrity.

Amini et al. (2011) explored how various EDM parameters, including Ip, V, *Ton*, and Toff, influence the surface roughness in the finishing stage when using a copper electrode on hot work steel DIN 1.2344. They employed a complete factorial design of experiments (DOE) for their analysis. After a thorough statistical evaluation, artificial neural networks (ANN) were applied to determine the optimal machining settings for achieving surface roughness. A hybrid model was also created to address any inaccuracies from the ANN. The results indicated that this approach effectively optimized complex and nonlinear challenges. Furthermore, the tool's geometry emerged as a crucial factor affecting both material flow during machining and the traverse rate of the process. Essentially, the tool serves two main functions: minimizing heat generation and facilitating material flow (El-Taweel et al., 2010).

Taguchi plays a vital role in the experimental design of Electric Discharge Machining (EDM) and laser EDM (μ-EDM), as well as in tackling both single and multi-objective optimization challenges in this field (Shivakoti et al., 2013). The outcomes show a notable improvement in productivity, surface finish, and wear of the electrodes (Ponappa et al., 2010). However, the complexity involved in Taguchi's multi-objective decision-making can lead to inefficiencies in its application. For instance, the overcut (OC) and taper angle (TA) in l-EDM for Gr304 were evaluated simultaneously using this method (Tamang et al., 2017). The

mathematical processes associated with it are quite intricate, and the determination of quality indicator weights relies purely on experimental data, which limits its practical effectiveness.

In EDM, various technological parameters are optimized for multiple objectives through Response Surface Methodology (RSM), focusing on metrics such as Material Removal Rate (MRR), Electrode Wear Rate (EWR), and OC (Ramaswamy & Perumal, 2020) (El-Taweel, 2009). Findings suggest that these parameters significantly impact quality, particularly when the T_{off} is at its lowest. This method proves suitable for addressing multi-objective challenges in EDM, revealing a maximum error margin of ±8% between theoretical predictions and experimental results. Furthermore, RSM, combined with Genetic Algorithms (GA), is utilized for multi-objective optimization in l-EDM for AISI SS304 (El-Taweel, 2009). The accuracy of the optimal results is quite satisfactory, with a maximum error of just 3.73%.

In another study, MRR, Tool Wear Rate (TWR), OC, and TA were concurrently analyzed for Ti-6Al-4V using the RSM-TOPSIS approach (Tiwary et al., 2014). The quality metrics achieved significant improvements under the best settings. Nonetheless, it has been observed that using RSM often requires a substantial number of tests with limited levels of specific technological parameters, and these levels are not selected randomly. This situation complicates the selection process for parameter levels in EDM. To improve efficiency in multi-objective optimization, Taguchi has been integrated with various multi-objective decision-making methodologies, including Artificial Neural Networks (ANN), Grey Relational Analysis (GRA), and Multi-Objective Genetic Algorithm II (MOGA-II), among others (Kumar et al., 2020; Nayim et al., 2019).

The MOGA-II method was utilized for multi-objective optimization in l-EDM focusing on the Ni-Ti alloy, with a selection of seven quality parameters: MRR, TWR, Ra, OC, TA, and circularity, as outlined in the study (Abidi et al., 2018). The results show a significant enhancement in the quality and characteristics of the machined surface under optimal conditions. Notably, the Tungsten electrode exhibits a lower TWR than the Cu electrode in l-EDM, improving machining precision. When evaluating the performance of different methods, MOGA offers a simultaneous assessment of RTL and SR in EDM for 316L steel, though the combined Taguchi – NSGA-II approach proves to be more efficient overall (Al-Amin eta l., 2021). The optimal results were achieved with an error margin below 10%. Despite the intricate nature of the computational method, multi-objective optimization using Taguchi methods has shown effectiveness, providing optimal and straightforward results (Kumar et al., 2020). The empirical establishment of quality criterion weights notably reduces the practical applicability of the ideal results. Additionally, Taguchi–ANN has been applied to enhance both the Material Removal Rate (MRR) and Surface Roughness (SR) in Electrical Discharge Machining (EDM) (Porwal et al., 2012; Bharti et al., 2012; El-Zathry et al., 2024).

The research findings suggest that Artificial Neural Networks (ANN) are a highly effective computational approach, achieving impressive accuracy. The maximum errors recorded for Material Removal Rate (MRR) and Surface Roughness (SR) were 4% and 4.67%, respectively. Similar procedures utilizing l-EDM with a WC electrode on Invar-36 demonstrated exceptional results; under optimal conditions, the MRR increased by 111%, while both the Tool Wear Rate (TWR) and Tool Life (TA) saw reductions of 38% and 45% (Manivannan & Kumar, 2017; Manivannan & Kumar, 2016). Moreover, seven quality criteria within μ-EDM were concurrently evaluated using the Taguchi-TOPSIS methodology, highlighting its efficiency in determining the set of technological parameters for μ-EDM (Manivannan & Kumar, 2017).

Compared to the TOPSIS method, the computational processes involving Genetic Algorithm (GA), Particle Swarm Optimization (PSO), and Grey Relational Analysis (GRA) for multi-objective decision-making are notably more intricate. The findings indicate that altering weights can lead to different results in multi-objective optimization challenges, showing a decrease in ideal efficiency within the application range. Principal Component Analysis (PCA) is employed to gauge the significance of the quality criteria in the multi-objective EDM scenario (Padhi et al., 2016; Chandrashekarappa et al., 2021; Meel et al., 2022). While the optimal outcomes are promising, the computation involved is quite complex.

The Analytic Hierarchy Process (AHP) provides a simpler method for evaluating the importance of quality indicators in electrical discharge machining (EDM). The results hold significant practical value, determining the ideal outcomes for MRR, TWR, and SR through ranking in the Topsis approach (Nadda et al., 2018). Signal-to-Noise (S/N) analysis in Topsis helps identify the best quality index in EDM, resulting in superior findings, which are crucial for μ-EDM research (Huo et al., 2019). There is a remarkable diversity of methodologies that derive optimal results across various studies, leading to outcomes that can be hard to apply. Furthermore, comparing MRR and Overcut (OC) in μ-EDM using a W electrode with workpieces made of copper, nickel, and copper-nickel revealed that copper exhibited the highest MRR, OC,

and surface quality, while nickel performed the poorest (Li et al., 2012; Padhi et al, 2016). The choice of workpiece material significantly affects optimization outcomes in μ-EDM, especially when considering its effectiveness in creating small apertures in titanium alloy workpieces (Apostolopoulou & Al-Juboori, 2019). In addressing complex objective problems, several methodologies such as Grey Relational Analysis (GRA) and the Technique for Order Preference by Similarity to Ideal Solution (TOPSIS) are available (Sabry et al., 2024c; Sabry & Hewidy, 2023; Sabry et al., 2022a; Sabry et al., 2020). Additional methods like hybrid GRA-TOPSIS, GRA based on the Taguchi method, and hybrid TOPSIS utilizing the Taguchi method offer versatile solutions to these multi-faceted challenges (Sabry et al., 2024; Sabry et al., 2024; Sabry et al., 2022; Sabry et al., 2021).

This work aims to study and improve the machining parameters in EDM of tungsten carbide on the machining characteristics. The characteristics of EDM refer essentially to output machining parameters such as material removal rate (MRR) and surface roughness (SR). The machining parameters are the input parameters of the EDM process, electrode rotational speed, peak current, and Pulse on time, to get a greater material removal rate.

Experimental work

The experiments used an electrical discharge machine, specifically the ELEKTRA 5535-EZNC EDM. We employed a custom rotary electrode attachment secured to the machine head for the rotary machining process. The project involved the creation of a Tungsten Carbide workpiece measuring 10 mm × 10 mm × 8 mm, intended for various applications such as pollution-control stack liners, ducts, dampers, scrubbers, and stack gas reheaters. Additionally, these components are useful in chemical processing setups like heat exchangers, reaction vessels, evaporators, transfer pipework, pharmaceuticals, food processing machinery, and marine engineering.

The rotating electrode was made from a brass-coated rod with a diameter of 4 mm. In Figure 1(a), you can see the machine setup used, where experiments were conducted on tungsten carbide flat samples with a thickness of 8 mm. The tool electrode utilized for these experiments was a brass-coated rod measuring 4 mm in diameter. Figure 1(b) illustrates the workpieces produced via the rotary EDM process and Figure 1(c) should be cited in the text.

The properties and composition of the Tungsten Carbide workpiece material are summarized in Table 1

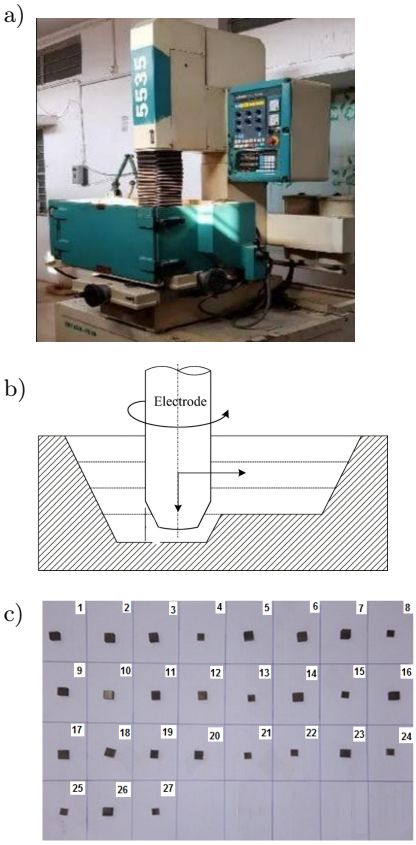

Fig. 1. Electronica Elektra Plus (a) EDM with rotary tool setup, (b) electrode rotary tool, (c) tungsten carbide workpieces after machining

and Table 2. To enhance the material removal rate (MRR), optimal settings for parameters such as electrode rotational speed, peak current, and Pulse on time were established. The effects of these four process factors on MRR and surface roughness (SR) during the EDM process are detailed in Tables 3 and 4.

Table 1
Tungsten Carbide chemical composition (weight percentage)

Element	W	C	Co	Ni	Cr	Ti	Ta	V
Weig.(%)	70	3	10	10	2	2	1	2

Table 2
Mechanical characteristics of the material used for the workpiece

Melting Point (°C)	Density (kg/m^3)	Poison's ratio ν	Young modulus (Mpa)
2870	15.7 g/cm^3	0.31	650

Table 3
Various control parameter levels

Parameter	Unit	Level		
		–1	0	1
Speed of rotational (N)	rpm	50	100	150
The current of Peak (I)	A 0.5	1.5	2	
pulse on time (Ton)	ms	3	6	9

Table 4
Experiments and a design matrix for full factorial analysis

Test Run	Factors			Performance parameter	
	N	Ip	Ton	MRR g/min	SR (Ra) µm
1	–1	1	–1	0.04420	1.4
2	–1	–1	–1	0.14610	2.8
3	1	–1	1	0.28810	3.9
4	–1	1	1	0.05130	1.2
5	0	0	0	0.15710	2.8
6	1	1	1	0.31340	3.8
7	1	1	–1	0.06410	1.7
8	–1	–1	1	0.24740	3.0
9	1	1	1	0.19850	3.1
10	–1	–1	–1	0.07911	2.3
11	1	–1	–1	0.12030	2.7
12	–1	–1	1	0.24490	3.6
13	1	–1	–1	0.06020	1.8
14	1	–1	–1	0.22990	3.1
15	–1	–1	1	0.18880	3.2
16	–1	1	–1	0.09089	1.9
17	1	1	1	0.13120	2.6
18	0	0	0	0.25060	3.5
19	1	–1	1	0.23810	3.2
20	1	1	–1	0.05750	2.0
21	–1	1	–1	0.16990	3.4
22	–1	–1	–1	0.08222	2.1
23	–1	1	1	0.26770	3.6
24	0	0	0	0.12220	2.6
25	1	–1	1	0.05990	1.0
26	1	1	–1	0.16910	2.7
27	–1	1	1	0.34490	3.7

Complete factorial Design of Experiments is a well-accepted approach for experimental design and is an effective strategy for enhancing process designs and solving production difficulties (Sabry, 2021). This approach efficiently demonstrates the link between the machining and performance parameters. Electrode Rotational Speed, Peak Current, and Pulse on Time are the machining parameters used for this experiment. Table 3 shows the machining condition and the number of levels of the specified parameters. Based on literature and prior research, the parameters with the most significant impact on the mechanical characteristics of comparable EDM were chosen, with their notations and units described in Table 3 (Wrzecionek et al., 2021; Ţîţu et al., 2023; Szałek et al., 2021; Pekarčíková et al., 2023). The entire factorial experiment was conducted using a central composite design matrix centred on the surface response methodology, incorporating three factorial design variables selected throughout three phases and 27 experimental coded conditions, as detailed in Table 4.

Mathematical models have been created to determine the EDM MRR and R.S. as a function of electrode rotating speed, peak current, and Pulse on time. $Y = f(I, N, T)$, where Y electrode rotational speed (N), peak current (I), and Pulse on time (T) are the variables. The selected polynomial may be written as

$$\mathrm{Y} = \mathrm{b0} + \mathrm{b1N} + b3I + b3T + b12N^{*}I + b13N^{*}T + b23I^{*}T \quad (1)$$

The coefficients for the linear terms b1, b2, and b3 and the interaction terms b12, b13, and b23 are for the three variables, where b0 is a constant. Regression analysis was used to ascertain the values of the polynomial equation. For statistical analysis, the Minitab program was utilized. The final mathematical models were produced and coded following the investigation.

The surface of a microrod can be defined by many factors, including arithmetical mean roughness (Ra). Arithmetical mean roughness, or Ra, is the predominant parameter, representing the arithmetic average of departures from the mean line. Maximum Peak refers to the distance between the highest and lowest valleys within a sampling length. To assess surface roughness, employ ImageJ, an image processing and analysis software with plugins for Measurement. The plugin Roughness_calculation.java calculates surface roughness statistics from a picture of the surface topology. Input an image or stack containing pixel values that denote the distance, z, to the surface. The plugin computes roughness metrics, including Ra. Utilize the Facet Orientation plugin (Sabry et al., 2019; Manivannan & Kumar, 2016; Padhi et al., 2016) to assess surface topography comprehensively.

Results and Discussion

The entire factorial analysis was conducted using the experimental data, considering SR and MRR. The Pareto chart obtained following the whole factorial analysis is shown in Figure 2.

Three factors – N, Ip, and Ton – were discovered to be important in calculating the MRR. According to the main effect graphs in Figure 3, MRR dramatically

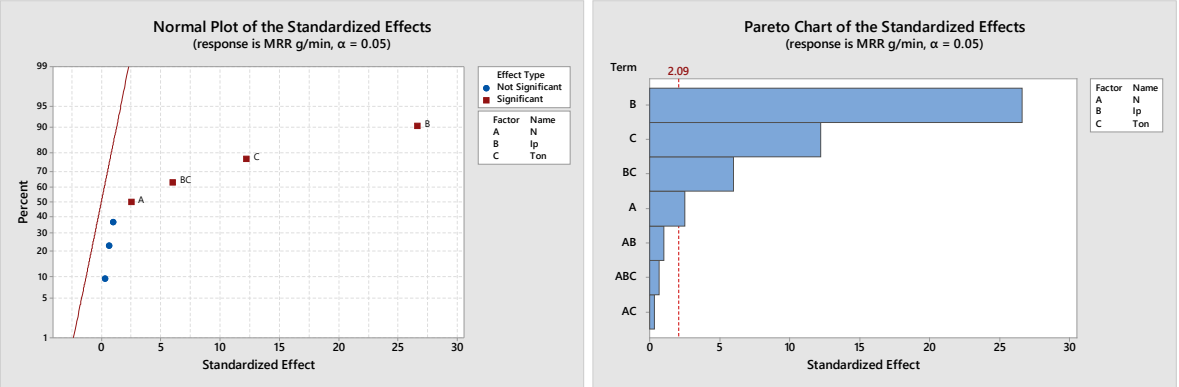

Fig. 2. Pareto chart Pareto chart and standard plot – MRR

increased as N and Ton rose from low to high. On the other hand, MRR increased when EDM was used at a slow travel speed. N, Ip and Ton had p-values of 0.005, 0.003, and 0.0050, respectively. The key factors were significant in a 95% confidence interval since their p-values were less than 0.05.

However, N^*Ip^*, N^*Ton, and N^*Ton interactions had p-values of 0.0984, 0.4521, and 0.0001, respectively. Interactions with p-values higher than 0.05 were insignificant in a 95 % confidence range. The interaction plot in Figure 4 showed parallel lines, suggesting that the two-way interactions were insignificant. Equation 1 provides a model to forecast the MRR. The model's R-sq value was 98.78%, meaning that factors and interactions accounted for 98.78% of the variance in the MRR.

$$\begin{aligned}
\text{MRR g/min} &= 0.1636 - 0.009370N_50 \\
&+ 0.000031N_100 \\
&+ 0.009339N_150 \\
&- 0.09812Ip_0.5 \\
&+ 0.009873Ip_1.5 \\
&+ 0.08825Ip_2.0 \\
&- 0.04292\,Ton_3 \\
&- 0.006138\,Ton_6 \\
&+ 0.04905\,Ton_9 \\
&+ 0.004149N^*Ip_50\ 0.5 \\
&+ 0.004048N^*Ip_50\ 1.5 \\
&- 0.008197N^*Ip_50\ 2.0 \\
&- 0.000949N^*Ip_100\ 0.5 \\
&- 0.003787N^*Ip_100\ 1.5 \\
&+ 0.004736N^*Ip_100\ 2.0 \\
&- 0.003200N^*Ip_150\ 0.5 \\
&- 0.000261N^*Ip_150\ 1.5 \\
&+ 0.003461N^*Ip_150\ 2.0 \\
&+ 0.000137N^*\,Ton_50\ 3 \\
&+ 0.001392N^*\,Ton_50\ 6 \\
&- 0.001529N^*\,Ton_50\ 9 \\
&+ 0.000036N^*\,Ton_100\ 3 \\
&+ 0.004158N^*\,Ton_100\ 6 \\
&- 0.004193N^*\,Ton_100\ 9 \\
&- 0.000172N^*\,Ton_150\ 3 \\
&- 0.005550N^*\,Ton_150\ 6 \\
&+ 0.005722N^*\,Ton_150\ 9 \\
&+ 0.02922Ip^*\,Ton_0.5\ 3 \\
&+ 0.001247Ip^*\,Ton_0.5\ 6 \\
&- 0.03047Ip^*\,Ton_0.5\ 9 \\
&- 0.006007Ip^*\,Ton_1.5\ 3 \\
&- 0.009918Ip^*\,Ton_1.5\ 6 \\
&+ 0.01592Ip^*\,Ton_1.5\ 9 \\
&- 0.02322Ip^*\,Ton_2.0\ 3 \\
&+ 0.008671Ip^*\,Ton_2.0\ 6 \\
&+ 0.01455Ip^*\,Ton_2.0\ 9 \\
&- 0.002516N^*Ip^*\,Ton_50\ 0.5\ 3 \\
&+ 0.000729N^*Ip^*\,Ton_50\ 0.5\ 6 \\
&+ 0.001787N^*Ip^*\,Ton_50\ 0.5\ 9 \\
&+ 0.000919N^*Ip^*\,Ton_50\ 1.5\ 3 \\
&- 0.007403N^*Ip^*\,Ton_50\ 1.5\ 6 \\
&+ 0.006484N^*Ip^*\,Ton_50\ 1.5\ 9 \\
&+ 0.001597N^*Ip^*\,Ton_50\ 2.0\ 3 \\
&+ 0.006674N^*Ip^*\,Ton_50\ 2.0\ 6 \\
&- 0.008271N^*Ip^*\,Ton_50\ 2.0\ 9 \\
&+ 0.000382N^*Ip^*\,Ton_100\ 0.5\ 3 \\
&- 0.003640N^*Ip^*\,Ton_100\ 0.5\ 6 \\
&+ 0.003258N^*Ip^*\,Ton_100\ 0.5\ 9 \\
&+ 0.001353N^*Ip^*\,Ton_100\ 1.5\ 3 \\
&- 0.000736N^*Ip^*\,Ton_100\ 1.5\ 6 \\
&- 0.000618N^*Ip^*\,Ton_100\ 1.5\ 9 \\
&- 0.001736N^*Ip^*\,Ton_100\ 2.0\ 3 \\
&+ 0.004376N^*Ip^*\,Ton_100\ 2.0\ 6 \\
&- 0.002640N^*Ip^*\,Ton_100\ 2.0\ 9 \\
&+ 0.002133N^*Ip^*\,Ton_150\ 0.5\ 3 \\
&+ 0.002911N^*Ip^*\,Ton_150\ 0.5\ 6 \\
&- 0.005044N^*Ip^*\,Ton_150\ 0.5\ 9 \\
&- 0.002272N^*Ip^*\,Ton_150\ 1.5\ 3 \\
&+ 0.008139N^*Ip^*\,Ton_150\ 1.5\ 6 \\
&- 0.005867N^*Ip^*\,Ton_150\ 1.5\ 9 \\
&+ 0.000139N^*Ip^*\,Ton_150\ 2.0\ 3 \\
&- 0.01105N^*Ip^*\,Ton_150\ 2.0\ 6 \\
&+ 0.01091N^*Ip^*\,Ton_150
\end{aligned} \tag{2}$$

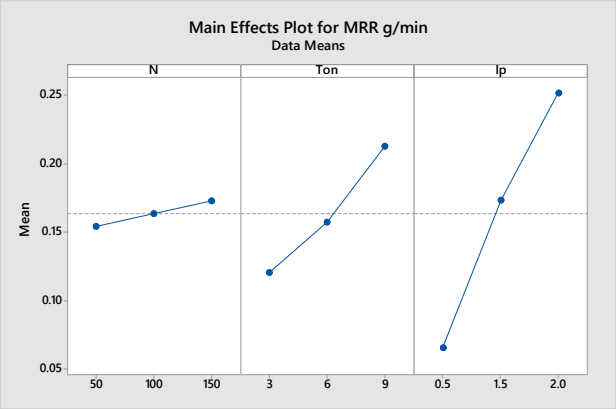

Fig. 3. Plot of main effects – MRR

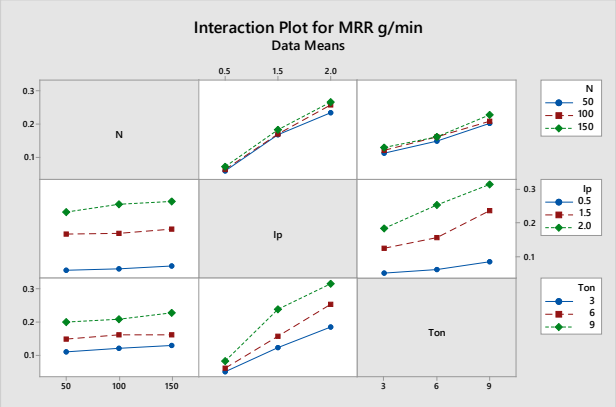

Fig. 4. Plotting the interaction effect – MRR

The chart for the SR is given in Figure 5. N, Ip, and Ton all had p-values of 0.000. Therefore, the SR considered three discrete parameters to be necessary. The primary effect plot in Figure 6 verified the conclusion. The findings agreed with those of the S.R. N^*Ip^*, N^*Ton, and N^*Ton had two-way interactions, and their p-values were 0.3679, 0.0035, and 0.0039, respectively. Therefore, no interactions had any bearing on SR, as shown in Figure 7. When N and Ton shifted from their corresponding low to high levels, the SR increased, whereas travel speed changed from high to low (Figure 9) – interaction effects of the parameters on the SR (2). The model's R-sq is 98.81%.

$$\begin{aligned}
\text{SR (Ra) } \mu\text{m} = {} & 2.693 + 0.1185N_50 \\
& - 0.003704N_100 \\
& - 0.1148N_150 \\
& - 0.9815Ip_0.5 \\
& + 0.1407Ip_1.5 \\
& + 0.8407Ip_2.0 \\
& - 0.3370\,Ton_3 \\
& + 0.02963\,Ton_6 \\
& + 0.3074\,Ton_9 \\
& + 0.07037N^*Ip_50\ 0.5 \\
& - 0.05185N^*Ip_50\ 1.5 \\
& - 0.01852N^*Ip_50\ 2.0 \\
& - 0.007407N^*Ip_100\ 0.5 \\
& + 0.003704N^*Ip_100\ 1.5 \\
& + 0.003704N^*Ip_100\ 2.0 \\
& - 0.06296N^*Ip_150\ 0.5 \\
& + 0.04815N^*Ip_150\ 1.5 \\
& + 0.01481N^*Ip_150\ 2.0 \\
& + 0.02593N^*\,Ton_50\ 3 \\
& - 0.04074N^*\,Ton_50\ 6 \\
& + 0.01481N^*\,Ton_50\ 9 \\
& - 0.01852N^*\,Ton_100\ 3 \\
& + 0.01481N^*\,Ton_100\ 6 \\
& + 0.003704N^*\,Ton_100\ 9 \\
& - 0.007407N^*\,Ton_150\ 3 \\
& + 0.02593N^*\,Ton_150\ 6 \\
& - 0.01852N^*\,Ton_150\ 9 \\
& - 0.1741Ip^*\,Ton_0.5\ 3 \\
& + 0.09259Ip^*\,Ton_0.5\ 6 \\
& + 0.08148Ip^*\,Ton_0.5\ 9 \\
& + 0.1370Ip^*\,Ton_1.5\ 3 \\
& - 0.09630Ip^*\,Ton_1.5\ 6 \\
& - 0.04074Ip^*\,Ton_1.5\ 9 \\
& + 0.03704Ip^*\,Ton_2.0\ 3 \\
& + 0.003704Ip^*\,Ton_2.0\ 6 \\
& - 0.04074Ip^*\,Ton_2.0\ 9 \\
& - 0.01481N^*Ip^*\,Ton_50\ 0.5\ 3 \\
& + 0.01852N^*Ip^*\,Ton_50\ 0.5\ 6 \\
& - 0.003704N^*Ip^*\,Ton_50\ 0.5\ 9 \\
& - 0.02593N^*Ip^*\,Ton_50\ 1.5\ 3 \\
& + 0.007407N^*Ip^*\,Ton_50\ 1.5\ 6 \\
& + 0.01852N^*Ip^*\,Ton_50\ 1.5\ 9 \\
& + 0.04074N^*Ip^*\,Ton_50\ 2.0\ 3 \\
& - 0.02593N^*Ip^*\,Ton_50\ 2.0\ 6 \\
& - 0.01481N^*Ip^*\,Ton_50\ 2.0\ 9 \\
& + 0.02963N^*Ip^*\,Ton_100\ 0.5\ 3 \\
& - 0.03704N^*Ip^*\,Ton_100\ 0.5\ 6 \\
& + 0.007407N^*Ip^*\,Ton_100\ 0.5\ 9 \\
& - 0.01481N^*Ip^*\,Ton_100\ 1.5\ 3 \\
& + 0.01852N^*Ip^*\,Ton_100\ 1.5\ 6 \\
& - 0.003704N^*Ip^*\,Ton_100\ 1.5\ 9 \\
& - 0.01481N^*Ip^*\,Ton_100\ 2.0\ 3 \\
& + 0.01852N^*Ip^*\,Ton_100\ 2.0\ 6 \\
& - 0.003704N^*Ip^*\,Ton_100\ 2.0\ 9 \\
& - 0.01481N^*Ip^*\,Ton_150\ 0.5\ 3 \\
& + 0.01852N^*Ip^*\,Ton_150\ 0.5\ 6 \\
& - 0.003704N^*Ip^*\,Ton_150\ 0.5\ 9 \\
& + 0.04074N^*Ip^*\,Ton_150\ 1.5\ 3 \\
& - 0.02593N^*Ip^*\,Ton_150\ 1.5\ 6 \\
& - 0.01481N^*Ip^*\,Ton_150\ 1.5\ 9 \\
& - 0.02593N^*Ip^*\,Ton_150\ 2.0\ 3 \\
& + 0.007407N^*Ip^*\,Ton_150\ 2.0\ 6 \\
& + 0.01852N^*Ip^*\,Ton_150\ 2.0\ 9
\end{aligned} \tag{3}$$

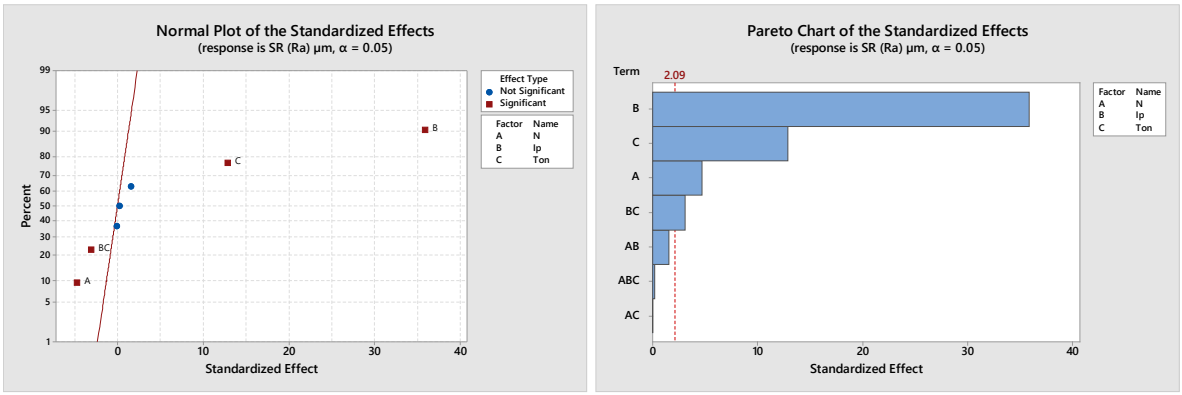

Fig. 5. Pareto chart Pareto chart and standard plot – SR

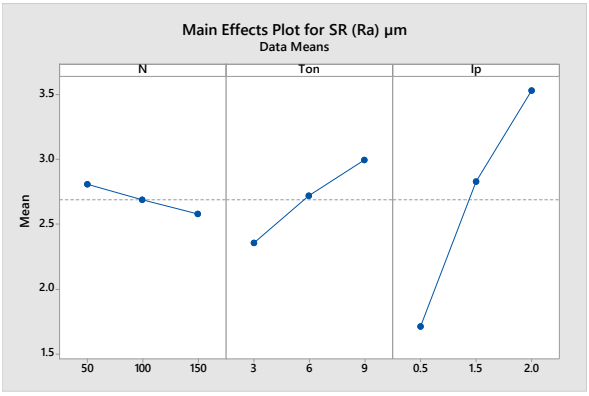

Fig. 6. Main effects plot – SR

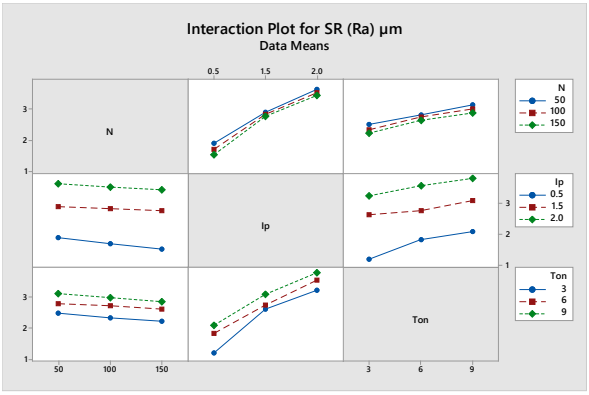

Fig. 7. Interaction effect plot – SR

This means that the increasing trend of MRR is higher at higher Ip and *Ton* than at lower *N* speed. The surface plot for MRR due to the interaction effect of the *N* and Ip is shown in Fig. 8(a,b,c). The surface plot for SR due to the *N* and *Ton* interaction effect is shown in Fig. 9(a,b,c). The decrease in SR is significant at larger *N*, while an insignificant decrease in SR at more minor *Ip* and *Ton* is observed.

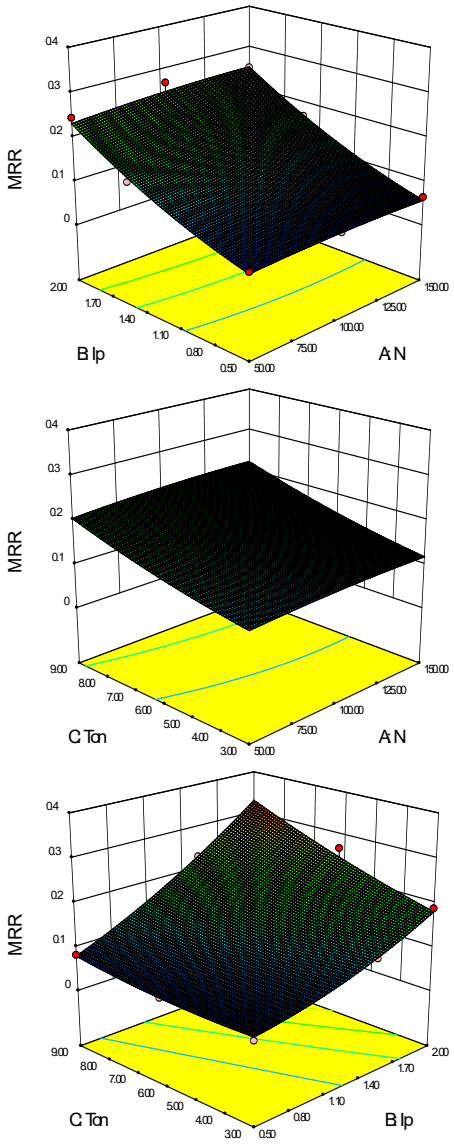

Fig. 8. Surface map showing how N, Ip, and *Ton* interact to affect MRR

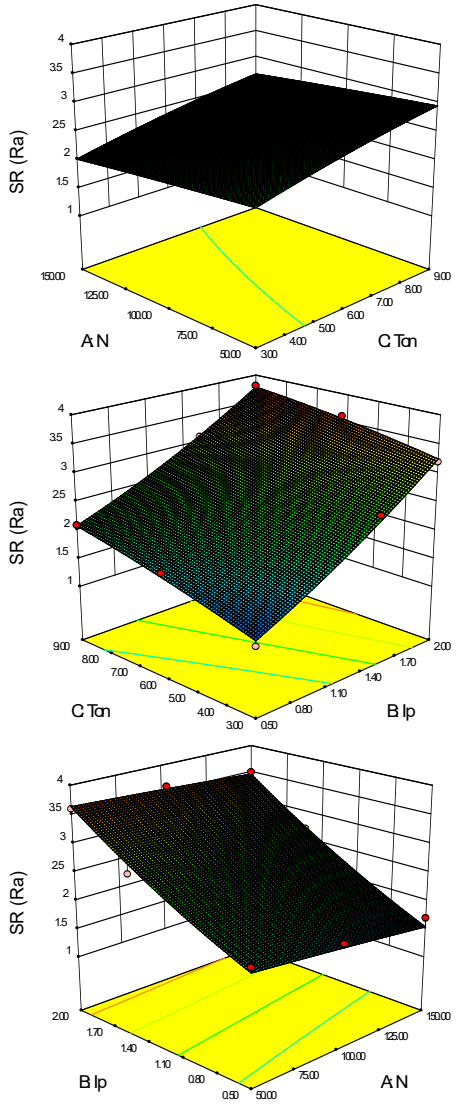

Fig. 9. Surface map showing how N, Ip, and *Ton* interact to affect SR

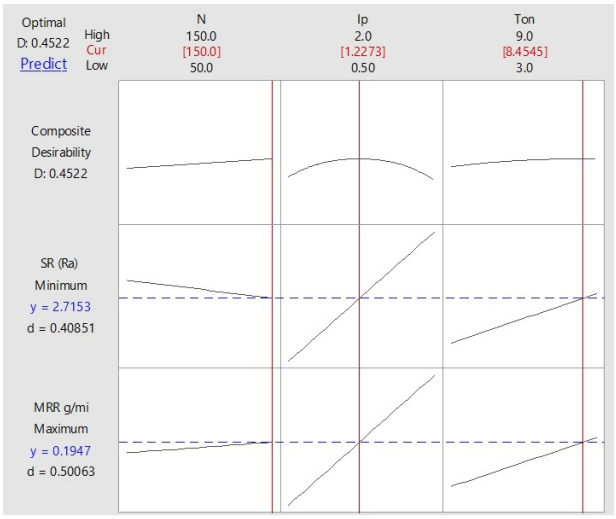

Fig. 10. Optimize the variables and responses in ANOVA by using the response optimizer

Figure 10 displays the optimized N, Ip, and Ton parameters and the matching MRR and SR response values from the ANOVA response optimizer. The ideal set of parameters for a single response or a collection of responses can be found using response optimizers. In this instance, various replies for the three input variables were optimized, and the result was an optimization plot. N, Ip, and Ton were each optimized at 150 rpm, 1.22 A, and 8.4 ms, respectively.

Discussion

In Electrical Discharge Machining (EDM), key process parameters such as peak current, Pulse on time, and rotational speed significantly impact surface roughness (SR) and material removal rate (MRR). Here's a detailed discussion of these effects:

Peak Current (Ip): Surface Roughness: Increasing the peak current often results in higher surface roughness. With a higher peak current, the discharge energy increases, leading to a more aggressive erosion process. This can cause larger craters on the workpiece surface, increasing roughness. Higher peak currents generally improve MRR by enhancing the energy per discharge, leading to faster material erosion. However, a current that is too high can also lead to a rougher finish and potentially reduce tool life due to excessive wear.

Pulse On-Time (*Ton*): Surface Roughness: Increasing the Pulse at 9 mm on time extends the duration each spark is in contact with the material, which can increase surface roughness as it causes deeper craters. However, a carefully optimized on-time can balance the roughness by controlling crater formation.

Material Removal Rate (MRR): A longer pulse on time improves MRR by allowing each discharge to remove more material. However, excessively long pulse durations may cause secondary discharges, potentially affecting surface quality and stability in material removal.

Rotational Speed (for Rotary EDM): Surface Roughness: In rotary EDM, where the electrode rotates during machining, higher rotational speeds at 150 rpm can improve surface finish. Rotation helps remove debris from the gap, providing better spark distribution and a finer surface. Material Removal Rate (MRR): Rotational speed enhances MRR by aiding debris evacuation and ensuring a consistent gap between the tool and workpiece. This consistent gap helps maintain steady discharges, improving machining efficiency.

In summary, optimizing these parameters – such as selecting a moderate peak current, controlling Pulse on time at 1.22 A, pulse *Ton* at 8.454 mms and using adequate rotational speed at 150 rpm – allows for a balance between achieving a smoother surface finish and maximizing MRR. The specific values, however, depend on the material properties and the desired machining outcome.

An analysis of variance was conducted to determine which factor significantly influenced the surface roughness and metal removal rate of micro rods produced via EDM. The ANOVA results for the surface roughness experimental data are presented in Fig. 2. and Fig. 5. The P-values are utilized to assess the statistical significance of each component. P-values below 0.05 signify that, at the 95% confidence level, capacitance,N^*, Ip, and *Ton* exert a statistically significant influence on surface roughness.

Conclusions

The EDM method worked well for tungsten carbide. It was discovered that the process parameters considerably impacted MRR and SR. Consequently, parameter optimization is crucial to achieving a strengthened EDM process. Below are the findings of the analysis using ANOVA.

1. In the 95 % confidence interval, the p values for the ANOVA's N^*Ip^*,N^*Ton, and N^*Ton interactions are less than 0.05. Thus, it has been established that the MRR is significantly influenced by the N, Ip, *Ton*, and the interplay of the current and N.
2. The relative p values for the N^*Ip^*,N^*Ton, and N^*Ton interactions, as well as the N-*Ton* interaction and the Ip-*Ton* interaction, are 0.3679, 0.0035, and 0.0039, 0.1036, 0.684, and 0.0664. In a 95 % confidence interval, every p-value is higher than 0.05.
3. Therefore, neither the principal effects of the parameters nor their interactions have any impact on the SR. The ANOVA-optimized values are 150 rpm, 1.22 A, and 8.4 ms. Regardless of the statistical analysis looked at, the outcomes based on these two analyses came to a single set of ideal values.
4. A mathematical model for surface roughness and metal removal rate employing dimensional analysis has been formulated by examining the process variables and the material characteristics that influence the surface roughness of micro rods produced by the EDM method.
5. The influence of input parameters on the surface roughness and metal removal rate of rods produced using EDM was examined using ANOVA.

References

Abidi, M.H., Al-Ahmari, A.M., Umer, U. and Rasheed, M.S. (2018). Multi-objective optimization of micro-electrical discharge machining of nickel-titanium-based shape memory alloy using MOGA-II. *Measurement*, 125, 336–349. DOI: 10.1016/J.MEASUREMENT.2018.04.096.

Al-Amin, M., Abdul-Rani, A.M., Ahmed, R. and Rao, T.V. (2021). Multiple-objective optimization of hydroxyapatite-added EDM technique for processing of 316L-steel. *Materials and Manufacturing Processes*, 36(10), 1134–1145. DOI: 10.1080/10426914.2021.1885715.

Amini, S., Atefi, R. and Solhjoei, N. (2011). The Influence of EDM Parameters in Finishing Stage on Surface Quality of Hot Work Steel Using Artificial Neural Network. *AIP Conf Proc*, 1315(1), 1228–1233. DOI: 10.1063/1.3552350.

Amorim F.L., and Weingaertner, W.L. (2007). The behaviour of graphite and copper electrodes on the finish die-sinking electrical discharge machining (EDM) of AISI P20 tool steel. *Journal of the Brazilian Society of Mechanical Sciences and Engineering*, 29(4), 366–371. DOI: 10.1590/S1678-58782007000400004.

Apostolopoulou, C. and Al-Juboori, L.A. (2019). Optimization of Micro-Electrical Discharge Machining Parameters of Ti6AL4V Component: A Mapping Study. *Journal of Mathematics Research*, 12(1), 22. DOI: 10.5539/JMR.V12N1P22.

Bharti, P.S., Maheshwari, S., & Sharma, C. (2010). Experimental investigation of Inconel 718 during die-sinking electric discharge machining. *International Journal of Engineering Science and Technology,* 2(11), 6464–6473 Available: https://www.researchgate.net/publication/50366320_Experimental_investigation_of_Inconel_718_during_die-sinking_electric_discharge_machining

Bharti, P. S., Maheshwari, S. and Sharma, C. (2012). Multi-objective optimization of electric-discharge machining process using controlled elitist NSGA-II. *Journal of Mechanical Science and Technology*, 26(6), 1875–1883. DOI: 10.1007/S12206-012-0411-X/METRICS.

Bhaumik, M. and Maity, K. (2019). Effect of deep cryotreated tungsten carbide electrode and SiC powder on EDM performance of AISI 304. *Particulate Science and Technology*, 37(8), 977–988. DOI: 10.1080/02726351.2018.1487491.

Chandrashekarappa, M.P., Kumar, S., Jagadish, G., Pimenov, D.Y. and Giasin, K. (2021). Experimental Analysis and Optimization of EDM Parameters on HcHcr Steel in Context with Different Electrodes and Dielectric Fluids Using Hybrid Taguchi-Based PCA-Utility and CRITIC-Utility Approaches. *Metals*, 11(419). DOI: 10.3390/MET11030419.

Chattopadhyay, K.D., Satsangi, P.S., Verma, S., & Sharma, P.C. (2008). Analysis of rotary electrical discharge machining characteristics in reversal magnetic field for copper-en8 steel system. *International Journal of Advanced Manufacturing Technology*, 38(9–10), 925–937. DOI: 10.1007/S00170-007-1149-Y/METRICS.

Chen, S.M. and Lee, L.W. (2010). Fuzzy multiple attributes group decision-making based on the interval type-2 TOPSIS method. *Expert Syst Appl*, 37(4), 2790–2798. DOI: 10.1016/J.ESWA.2009.09.012.

Dinesh, D., Sangaravadivel, P., Jeevith, R., Kishore, M., Deepith, N. & Srikanth, M. (2024). Investigation of Inconel 718 on Electrical Discharge MachiningUsing Copper and Copper Alloy-Tungsten Disulfide Electrodes. *SAE Technical Papers*. DOI: 10.4271/2023-01-5149.

El-Taweel, T.A. (2009). Multi-response optimization of EDM with Al-Cu-Si-TiC P/M composite electrode. *International Journal of Advanced Manufacturing Technology*, 44(1–2), 100–113. DOI: 10.1007/S00170-008-1825-6/METRICS.

El-Taweel, T.A., Youssef, A.H. and Hewidy, A.M. (2010). Optimum selection of wedm conditions for ck45 steel. *ERJ. Engineering Research Journal*, 33(3), 297–306. DOI: 10.21608/ ERJM.2010.67331.

El-Zathry, N.E., Akinlabi, S., Woo, W.L. (2024). Friction Stir-Based Techniques: An Overview. *Weldin in the World*, 69, 327–361.

Huo, J., Liu, S., Wang, Y., Muthuramalingam, T. and Ngoc Pi, V. (2019). Influence of process factors on surface measures on electrical discharge machined stainless steel using TOPSIS. *Mater Res Express*, 6(8), 086507. DOI: 10.1088/2053-1591/AB1AE0.

Khudhir, W.S., Ahmed, B.A., & Shukur, J.J. (2024). Experimental investigation and optimization of surface roughness and kerf width in wire-EDM process. *AIP Conf Proc*, 3002(1). DOI: 10.1063/5.0206629/3297529.

Kumar, S., Thirupathi, N. and Saraswathamma, K. (2020). Experimental Investigation and Multi-Objective Optimization of Die sink EDM Process Parameters on Inconel-625 alloy by using Utility Function Approach. *Mater Today Proc*, 24, 995–1005. DOI: 10.1016/J.MATPR.2020.04.412.

Lee, S.H. and Li, X.P. (2001). Study of the effect of machining parameters on the machining characteristics in electrical discharge machining of tungsten carbide. *Journal of Material Processing Technology*, 115(3), 344–358. DOI: 10.1016/S0924-0136(01)00992-X.

Li, J., Shen, F. and Guo, M. (2012). Influence of Material Microstructure on Micro EDM. *Applied Mechanics and Materials*, 130–134, 927–930. DOI: 10.4028/www.scientific.net/amm.130-134.927.

Manikandan, R. and Venkatesan, R. (2012). Optimizing the machining parameters of micro-EDM for Inconel 718. *Journal of Applied Sciences*, 12(10), 971–977. DOI: 10.3923/JAS.2012.971.977.

Manivannan R. and Kumar, M.P. (2017). Multi-attribute decision-making of cryogenically cooled micro-EDM drilling process parameters using TOPSIS method. *Materials and Manufacturing Processes*. DOI: 10.1080/10426914.2016.1176182.

Manivannan R. and Kumar, M.P. (2016). Multi-response optimization of Micro-EDM process parameters on AISI304 steel using TOPSIS. *Journal of Mechanical Science and Technology*, 30(1), 137–144. DOI: 10.1007/S12206-015-1217-4/METRICS.

Meel, R., Singh, V., Katyal, P. and Gupta, M. (2022). Optimization of process parameters of micro-EDD/EDM for magnesium alloy using Taguchi based GRA and TOPSIS method. *Mater Today Proc*, 51, 269–275. DOI: 10.1016/J.MATPR.2021.05.287.

Nadda, R., Kumar, R., Singh, T., Chauhan, R., Patnaik, A. and Gangil, B. (2018). Experimental investigation and optimization of cobalt bonded tungsten carbide composite by hybrid AHP-TOPSIS approach. *Alexandria Engineering Journal*, 57(4), 3419–3428. DOI: 10.1016/J.AEJ.2018.07.013.

Naeim, N., AbouEleaz, M.A., & Elkaseer, A. (2023). Experimental Investigation of Surface Roughness and Material Removal Rate in Wire EDM of Stainless Steel 304. *Materials 2023*, 16(3), 1022. DOI: 10.3390/MA16031022.

Nayim, S.M., Hasan, M.Z., Jamwal, A., Thakur, S. and Gupta, S. (2019). Recent trends & developments in optimization and modelling of electro-discharge machining using modern techniques: A review. *AIP Conf Proc*, 2148(1). DOI: 10.1063/1.5123973/906677.

Padhi, P.C. Mahapatra, S.S. Yadav, S.N. and Tripathy, D.K. (2016). Multi-Objective Optimization of Wire Electrical Discharge Machining (WEDM) Process Parameters Using Weighted Sum Genetic Algorithm Approach. *https://doi.org/10.1142/S0219686716500086*, 15(2), 85–100. DOI: 10.1142/S0219686716500086.

Pekarčíková M.(2023). Case Study: Testing the Overall Efficiency of Equipment in the Production Process in TX Plant Simulation Software. *Management and Production Engineering Review*, 14(1), 34–42. DOI: 10.24425/MPER.2023.145364.

Ponappa, K., Aravindan, S., Rao, P.V., Ramkumar, J. and Gupta, M. (2010). The effect of process parameters on machining of magnesium nano alumina composites through EDM. *International Journal of Advanced Manufacturing Technology*, 46(9–12), 1035–1042. DOI: 10.1007/S00170-009-2158-9/METRICS.

Porwal, R.K., Yadava, V. and Ramkumar, J. (2012). Artificial neural network modelling and multi-objective optimization of hole drilling electro discharge micromachining of invar. *International Journal of Mechatronics and Manufacturing Systems*, 5(5–6), 470–494. DOI: 10.1504/IJMMS.2012.049974.

Ramaswamy, A. and Perumal, A.V. (2020). Multi-objective optimization of drilling EDM process parameters of LM13 Al alloy–10ZrB2–5TiC hybrid composite using RSM. *Journal of the Brazilian Society of Mechanical Sciences and Engineering*, 42(8), 1–18. DOI: 10.1007/S40430-020-02518-9/METRICS.

Rao, P.S., Ramji, K., & Satyanarayana, B. (2014). Experimental Investigation and Optimization of Wire EDM Parameters for Surface Roughness, MRR and White Layer in Machining of Aluminium Alloy. *Procedia Materials Science*, 5, 2197–2206, Jan. 2014. DOI: 10.1016/J.MSPRO.2014.07.426.

Sabry, I., El-Kassas, A.M., Mourad, A.-H.I., Thekkuden, D.T. and Qudeiri, Ja.A. (2019). Friction Stir Welding of T-Joints: Experimental and Statistical Analysis. *Journal of Manufacturing and Materials Processing,* 3(38), 1–23.

Sabry, I., Mourad, A.H.I. and Thekkuden, D.T. (2020). Optimization of metal inert gas-welded aluminium 6061 pipe parameters using analysis of variance and grey relational analysis. *SN Appl Sci*, 2(2), 1–11, Feb. 2020. DOI: 10.1007/S42452-020-1943-9/FIGURES/8.

Sabry, I. Idrisi, A.H. Mourad, A.-H.I. Sabry, I. Idrisi, A.H. and Mourad, A.-H.I. (2021a). Friction Stir Welding Process Parameters Optimization Through Hybrid Multi-Criteria Decision-Making Approach. *International Review on Modelling and Simulations (IREMOS)*, 14(1), 32–43. DOI: 10.15866/IREMOS.V14I1.19537.

Sabry, I. (2021b). Experimental and statistical analysis of possibility sources – rotation speed, clamping torque and clamping pith for quality assessment in friction stir welding. *Management and Production Engineering Review*, 12(3), 84–96. DOI: 10.24425/MPER.2021.138533.

Sabry, I., Thekkuden, T., Mourad, D., and Husain Khan, S. (2022a). Optimization of Tungsten Inert Gas Welding Parameters using Grey Relational Analysis for joining AA 6082 Pipes. *2022 Advances in Science and Engineering Technology International Conferences, ASET 2022*. DOI: 10.1109/ASET53988.2022.9735100.

Sabry I., Thekkuden, D.T. and Mourad, A.H.I. (2022b). TOPSIS – GRA Approach to Optimize Friction Stir Welded Aluminum 6061 Pipes Parameters. *Advances in Science and Engineering Technology International Conferences, ASET 2022*. DOI: 10.1109/ASET53988.2022.9734821.

Sabry I. and Hewidy, A.M. (2023). Multi-Weld Quality Optimization of Gas Tungsten Arc Welding for Aluminium 6061 using the Grey Relation Analysis-Based Taguchi Method. *Journal of Advanced Research in Applied Sciences and Engineering Technology*, 36(1), 26–42. DOI: 10.37934/ARASET.36.1.2642.

Sabry, I. Hewidy, A.M. Alkhedher, M. and Mourad, A.H.I. (2024b). Analysis of variance and grey relational analysis application methods for the selection and optimization problem in 6061-T6 flange friction stir welding process parameters. *International Journal of Lightweight Materials and Manufacture*, 7(6), 773–792. DOI: 10.1016/J.IJLMM.2024.06.006.

Sabry, I. Hewidy, A.M. Naseri, M. and Mourad, A.H.I. (2024c). Optimization of process parameters of metal inert gas welding process on aluminium alloy 6063 pipes using Taguchi-TOPSIS approach. *Journal of Alloys and Metallurgical Systems*, 7, 100085. DOI: 10.1016/J.JALMES.2024.100085.

Shivakoti, I., Kibria, G., Diyaley, S. and Pradhan, B.B. (2013). Multi-objective optimization and analysis of electrical discharge machining process during micro-hole machining of D3 die steel employing salt mixed de-ionized water dielectric. *Journal of Computational & Applied Research in Mechanical Engineering (JCARME)*, 3(1), 27–39. DOI: 10.22061/JCARME.2013.57.

Szałek, A. Szukiewicz, M. and Chmiel-Szukiewicz, E. (2021). Kinetic investigations of heterogeneous reactor processes – Optimization of experiments. *Chemical and Process Engineering – Inzynieria Chemiczna i Procesowa*, 42(1), 35–41. DOI: 10.24425/CPE.2021.137337.

Tamang, S.K. Natarajan, N. and Chandrasekaran, M. (2017). Optimization of EDM process in machining micro holes for improvement of hole quality. *Journal of the Brazilian Society of Mechanical Sciences and Engineering*, 39(4), 1277–1287. DOI: 10.1007/S40430-016-0630-7/METRICS.

Ţîţu, A.M., Pop, A.B. and Nabiałek, M. (2023). Modelling the natural gas transportation process using the factorial experiment method. *Archives of Metallurgy and Materials*, 68(3), 961–966. DOI: 10.24425/AMM.2023.145460.

Tiwary, A.P., Pradhan, B.B. and Bhattacharyya, B. (2014). Application of multi-criteria decision-making methods for selection of micro-EDM process parameters. *Adv Manuf*, 2(3), 251–258. DOI: 10.1007/S40436-013-0050-1/TABLES/10.

Wrzecionek, M. Howis, J. Marek, P.H. Ruśkowski, P. and Gadomska-Gajadhur, A. (2021). The catalyst-free polytransesterification for obtaining linear PGS optimized with use of 22 factorial design. *Chemical and Process Engineering – Inzynieria Chemiczna i Procesowa*, 42(1), 43–52, 2021. DOI: 10.24425/CPE.2021.137338.

Yan, B.H., Wang, C.C., Liu, W.D., & Huang, F.Y. (2000). Machining characteristics of Al2O3/6061Al composite using rotary EDM with a disklike electrode. *International Journal of Advanced Manufacturing Technology*, 16(5), 322–333. DOI: 10.1007/S001700050164/METRICS.